Motion Estimation/Compensated Compressed Sensing using Patch-Based Low Rank Penalty

Huisu Yoon and Jong Chul Ye

KAIST, 291 Daehak-ro, Yuseong-gu, Daejeon 305-701, Republic of Korea

ABSTRACT

In this paper, a novel patch-based signal processing algorithm for motion estimated/compensated compressed sensing dynamic MR imaging is proposed. More specifically, we impose a non-convex patch-based low-rank penalty that exploits self-similarities within the images. This penalty is shown to favor capturing geometric features such as edges rather than reconstructing the background noises. To solve the resulting non-convex optimization problem, we propose a globally convergent concave-convex procedure (CCCP) using convex conjugate, which has closed form solution at each sub-iteration. Experimental results demonstrate that the proposed algorithm outperforms the existing ones.

Keywords: Compressed sensing, motion estimation/compensation, dynamic cardiac imaging, k-t FOCUSS, patch, low-rank, CCCP

1. INTRODUCTION

MR imaging is an inherently slow imaging modality and this limitation is very critical especially for high resolution dynamic cardiac imaging. To address this issue, many researchers have recently applied compressed sensing (CS) approaches for dynamic imaging applications.[1] Compressed sensing (CS) tells us that accurate reconstruction is possible as long as nonzero support is sparse and sampling basis are incoherent.[2] For example, as dynamic images can be effectively sparsified in transform domain thanks to temporal redundancy, k-t FOCUSS[3] imposes sparsity constraint in a transform domain. Several sparsifying transform have been proposed in k-t FOCUSS framework.

Recently, patch-based regularization algorithms which exploit self-similarity within images have been investigated quite extensively among MR community. For example, Ravishankar and Bresler applied a dictionary learning algorithm for static MRI reconstruction,[4] whereas Akçakaya *et al.* applied collaborative filtering for cardiac MR application.[5] To incorporate nonlocal means algorithm, Yang *et al.* proposed a variational framework in compressed sensing MR reconstruction.[6–8] Extending the idea of calibration free parallel imaging using low-rank properties, Trzasko *et al.* recently introduced a patch based generalization algorithms for calibration free parallel imaging and dynamic imaging.[9]

By extending the prior works, this paper is interested in exploiting the self-similarities in spatiotemporal direction. In particular, this paper is interested in patch-based low rank constraint from similarity patches[10] since rank structures are relatively less sensitive to global intensity changes but easier to capture edges and etc. To achieve the goal, the proposed algorithm provides a two step hierarchical approach. More specifically, we perform a novel patch-based non-local ME/MC using a diastole phase reconstruction for initial image reconstruction, after which the patch-based low rank penalty is applied to improve the image quality. This is because a patch-based nonlocal ME/MC scheme can effectively remove the coherent aliasing artifacts and recover most of the dominant signal components, after which the patch based low rank penalty effectively capture geometric similarities such as edges and boundaries from aliasing free signals. In addition, unlike the existing patch-based processing for MR, we employ a non-convex rank proxy proposed in[11] due to its excellent performance. To deal with non-smooth and non-convex regularization terms, we propose a novel globally convergent concave-convex procedure (CCCP).[12] The resulting algorithm is a special case of majorize-minimize (MM) procedure, and does not require

Further author information: (Send correspondence to Jong Chul Ye)
Jong Chul Ye: E-mail: jong.ye@kaist.ac.kr, Telephone: +1-82-42-350-4360
Huisu Yoon.: E-mail: tea@kaist.ac.kr, Telephone: +1-82-42-350-4360

Wavelets and Sparsity XV, edited by Dimitri Van De Ville, Vivek K. Goyal, Manos Papadakis,
Proc. of SPIE Vol. 8858, 88581Y · © 2013 SPIE · CCC code: 0277-786X/13/$18
doi: 10.1117/12.2023170

any additional memory for storing Lagrangian parameters, which makes the algorithm suitable for memory bandwidth limited parallel implementation. Furthermore, each subprogram has a closed form solution, which can be easily accelerated. Our results demonstrate that patch-based low-rank regularization can effectively recover signals around important anatomical structures from highly undersampled measurements. Comparison with other state-of-the art algorithms show that the proposed algorithm is competitive and has advantages in dynamic region reconstruction. The organization of this paper is as follows. Details of the proposed algorithm is presented in section 2. Section 3 shows the experimental results. Finally, section 4 gives concluding remarks.

2. THEORY

2.1 Problem Formulation

Let $\mathbf{y} \in \mathbb{C}^{mT}$ and $\mathbf{x} \in \mathbb{C}^{nT}$ denote a vectorized spatiotemporal k-space measurement and an unknown image, respectively. Here, m, n and T denote the number of k-space samples, pixels of image frame, and temporal frames, respectively. Then, a forward model for dynamic MR imaging problem is given by

$$\mathbf{y} = F\mathbf{x} + \mathbf{w} \tag{1}$$

and $\mathbf{w}$ denotes the measurement noise, and F denotes a spatiotemporal Fourier sensing matrix.

Then, our imaging problem can be represented as

$$\mathcal{C}\left(\mathbf{d}\right) = \frac{1}{2}\|\mathbf{y} - F\mathbf{x}\|_F^2 + \Psi(\mathbf{x}) \tag{2}$$

where $\Psi(\mathbf{x})$ denotes a spatiotemporal low-rank patch penalty for unknown image $\mathbf{x}$.

2.2 Initialization Strategy

To use patch-based low-rank penalty, similar patches in the image $\mathbf{x}$ need to be grouped under similarity mapping. However, in our algorithm, $\mathbf{x}$ is the very object to be estimated. To address this issue, we iteratively update similarity mapping and the unknown image $\mathbf{x}$. More details are described in subsection 2.3. Because of this refinement scheme, we need an accurate initial image $\mathbf{x}_0$ for fast convergence. As an example for an initialization, recall ME/MC technique in video coding that uses motion vectors to exploit the temporal redundancies between frames. Jung *et al.*[3] employed a overlapped block motion compensation (OBMC), where a multiple ME blocks are overlapped during compensation. By extending the OBMC, we are interested in minimizing the following *apodized* cost function and used the following fixed point update:

$$\mathcal{R}_p\mathbf{m} = \frac{\sum_{i\in\mathcal{N}_p} \mathcal{R}_i\mathbf{r}_c \exp\left(-\frac{\|\mathcal{R}_p\mathbf{m}^{(0)} - \mathcal{R}_i\mathbf{r}\|^2}{h}\right)}{\sum_{i\in\mathcal{N}_p} \exp\left(-\frac{\|\mathcal{R}_p\mathbf{m}^{(0)} - \mathcal{R}_i\mathbf{r}\|^2}{h}\right)} \,. \tag{3}$$

As we allow the overlapping of the patches, the overlapped pixel values are averaged after the fixed point iteration. After performing motion compensation (3), the residual image is reconstructed using k-t FOCUSS, and the final image is obtained adding the motion compensated image and reconstructed residual signal. Then, the final image is used as an initialization for the proposed algorithm. Hereafter, we call this k-t FOCUSS with the modified ME/MC scheme as k-t FOCUSS with NLMC (nonlocal motion compensation).

2.3 Optimization Framework

Let $\mathcal{R}_{pq} : \mathbf{x} \mapsto \mathcal{R}_{pq}\mathbf{x} \in \mathbb{C}^B$ denote an operator that extracts a vectorized version of a B-pixel square patch from an image frame in $\mathbf{x}$; and p and q denote the indices for a reference patch and its corresponding similar patches, respectively, where $p = 1, \cdots, P; q = 1, \cdots, Q$. Then, for the current block $\mathbf{v}_{p1} = \mathcal{R}_{p1}\mathbf{x}$, we search similarity patches $\{\mathbf{v}_{pq}\}_{q=2}^{Q_p}$ within the 3D neighborhood to construct a matrix

$$V_p = [\mathcal{R}_{p1}\mathbf{x}, \quad \mathcal{R}_{p2}\mathbf{x}, \quad \cdots, \quad \mathcal{R}_{pQ_p}\mathbf{x}] \in \mathbb{R}^{B\times Q_p}. \tag{4}$$

Then the constraint term can be written using the following rank penalty:

$$\Psi(\mathbf{x}) = \lambda \sum_p \text{Rank}(V_p). \tag{5}$$

One of the popular convex relaxation for the rank function is given by the nuclear norm.[10] However, as it has been shown that concave penalty outperforms that convex nuclear norm,[11] we use the following rank prior[11]

$$\|V_p\|_\nu = \sum_{k=1}^{\text{Rank}(V_p)} h_{\mu,\nu}\left(\sigma_k(V_p)\right), \quad 0 < \nu \leq 1. \tag{6}$$

where the generalized Huber function $h_{\mu,\nu}(t)$ is defined as

$$h_{\mu,\nu}(t) = \begin{cases} |t|^2/2\mu, & \text{if } |t| < \mu^{1/(2-\nu)} \\ |t|^\nu/\nu - \delta & \text{if } |t| \geq \mu^{1/(2-\nu)} \end{cases} \tag{7}$$

and $\delta = (1/\nu - 1/2)\mu^{\nu/(2-\nu)}$ to make the function continuous. Then, the resulting regularization for the residual is given by

$$\Psi(\mathbf{x}) = \lambda \sum_p \|V_p(\mathbf{x})\|_\nu. \tag{8}$$

For the generalized Huber function in Eq. (7), even though it is not convex by itself, it is easy to show that $|t|^2/\mu - h_{\mu,\nu}(t)$ is strictly convex. Therefore, the Legendre-Fenchel transform tells us that there exist $g_{\mu,\nu}$ such that

$$h_{\mu,\nu}(t) = \min_s \{|s-t|^2/\mu + g_{\mu,\nu}(s)\} \ . \tag{9}$$

The corresponding rank penalty for a matrix V is given by

$$\begin{aligned} \|V\|_{h_{\mu,\nu}} &= \sum_{k=1} h_{\mu,\nu}(\sigma_k(V)) \\ &= \min_W \left\{ \frac{1}{\mu}\|V-W\|_F^2 + \|W\|_{g_{\mu,\nu}} \right\} \end{aligned} \tag{10}$$

where

$$\|W\|_{g_{\mu,\nu}} = \sum_{k=1} g_{\mu,\nu}(\sigma_k(V)). \tag{11}$$

Using Eq. (10), the resulting cost function is given by

$$\begin{aligned} \mathcal{C}(W,\mathbf{x}) = \sum_{c=1}^{C} \|\mathbf{y}_c - F\mathbf{x}_c\|^2 \\ +\lambda \sum_p \min_W \left\{ \frac{1}{\mu}\|V_p(\mathbf{x}) - W_p\|_F^2 + \|W_p\|_{g_{\mu,\nu}} \right\} \end{aligned} \tag{12}$$

One of the main advantages of the proposed CCCP framework is that each subproblem has close form solutions. First, note that the problem can be decomposed into individual patches. Therefore, for a given estimate of $V_p^{(k)}$, we need to solve the following minimization problem:

$$W_p^{(k+1)} = \arg\min_W \left\{ \frac{1}{\mu}\|V_p^{(k)} - W\|_F^2 + \|W\|_{g_{\mu,\nu}} \right\} \ . \tag{13}$$

Even though $g_{\mu,\nu}(s)$ in Eq. (11) is not convex for $\nu < 1$ and does not have close form expression, there exist a close form expression for the minimizer of Eq. (9) given as[11,13]

$$\text{shrink}_\nu(t,\mu) := \arg\min_s\{|s-t|^2/\mu + g_{\mu,\nu}(s)\} = \max\{0, |t| - \mu|t|^{\nu-1}\}t/|t| \ . \quad (14)$$

If $V_p^{(k)}$ has a singular value decomposition $V_p^{(k)} = L\Sigma U^H$, then the closed form solution for Eq. (13) is given by

$$W_p^{(k+1)} = L \ \text{shrink}_\nu(\Sigma,\mu) \ U^H. \quad (15)$$

Next step is to find a closed form expression for the minimization of Eq. (12) with respect to $\mathbf{x}_c$. This can be done easily using conjugate gradient method. In our CCCP framework, we nearly solve $\mathbf{x}$ using conjugate gradient step, after which SVD is applied. This makes the proposed algorithm converges faster than FISTA based low rank penalty, in which SVD computation is needed for every gradient step. Similar observations have been made using alternative directional method of multiplier (ADMM) or alternating augmented Lagrangian method (ALM).[14]

3. RESULTS

We compared k-t FOCUSS, k-t FOCUSS with NLMC, k-t SLR, and the proposed algorithm. k-t SLR algorithm exploits global low-rank structure of spatiotemporal image.[15] Specifically, a spatiotemporal image is restructed as a matrix to solve the matrix recovery problem with low-rank penalty. A sparsity prior is also used to improve the reconstruction quality.

3.1 Simulation data

Simulation data is a MCAT phantom which mimics a dynamic heart motion. We used the program by Segars *et al.*[16,17] It contains left and right ventricle structures and shows systole and diastole phase dynamics. The matrix size is 128 × 128, and the number of time frames is 50. The data was corrupted by 33.8dB Gaussian noise. Downsampling rate was 6.1. Fig 1 shows the results. The first row shows 13th frame images and the second row shows 80th temporal profile images. (a) and (b) represent the ground truth. Results of k-t FOCUSS with NLMC is shown in (b) and (f) and k-t SLR results in (c) and (g). Results from both algorithms show retaining aliasing artifacts near edges, especially for valve structures. These are indicated by arrows. However, in (d) and (h), the proposed algorithm shows smoother edges than other algorithms and the valve shapes are clearly observed.

Fig 2 represents quantitative measures of the algorithms. In Fig. 2(a), k-t FOCUSS with motion compensation improves k-t FOCUSS. k-t SLR shows lower MSE that motion compensated k-t FOCUSS. The proposed algorithms shows the lowest MSE. In order to confirm the importance of initialization for refinable similarity search scheme, different initial images were tested. This is represented in Fig. 2(b). Here, we can see that initialization by k-t FOCUSS with NLMC was the first to achieve the lowest MSE. Also the lowest MSE value of that case is lower than other two. This is because the proposed algorithm deals with non-convex surrogate function of non-convex penalty. Although this scheme does not guarantee global minimum, it goes to better local minima with faster convergence rate as shown in Fig. 2(b).

3.2 Real experiment

We did the same experiment for real *in vivo* data. A real cardiac cine data set was acquired using a 1.5 T Philips scanner at Yonsei University Medical Center, Korea: the acquisition sequence is bSSFP, with a flip angle of 50^o. The heart rate of the subject was 75 bpm. The imaging parameters were as follows: FOV is 345 × 270 mm^2, the matrix size is 256 × 256, TR is 3.17 ms, the number of cardiac phases is 25. Downsampling rate was 8.

Fig. 3 shows the results of algorithms. The first row shows region of interest (ROI) image, and the second row shows temporal profile images. As can be seen in (a) and (e), the ground truth includes considerable noise. In (b), k-t FOCUSS with NLMC shows low denoising quality in ROI, and temporal aliasing artifacts still remaining in (f). k-t SLR shows highly denoised image from (c) and (g). However, edge structure was not

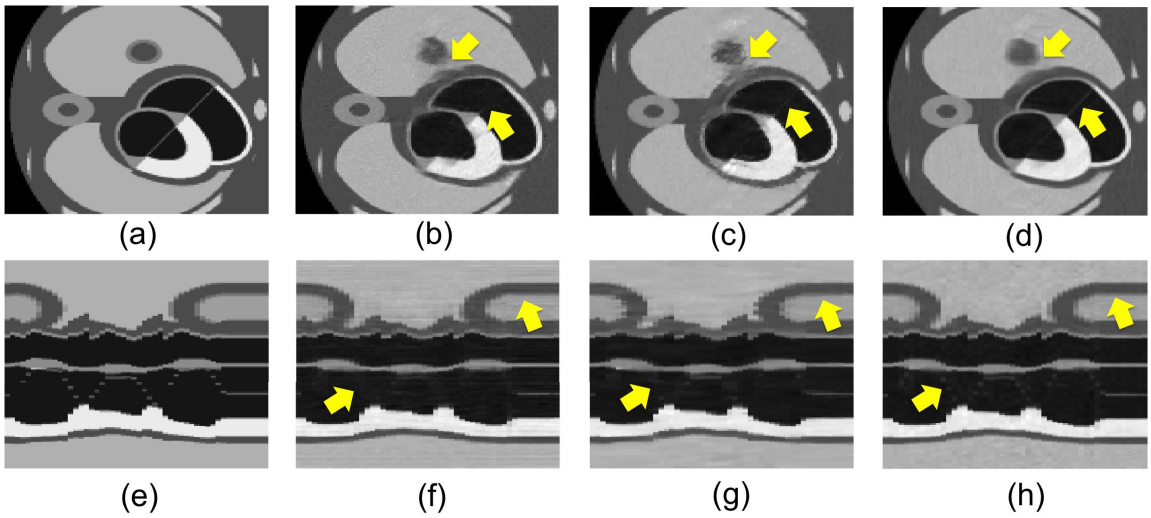

Figure 1: Reconstruction results of MCAT dynamic cardiac phantom with 33.8dB Gaussian noise. The k-space data was obtained in cartesian coordinates, and the acceleration ratio was x6.1. First row represents the 13th frame images of (a) the ground-truth, reconstruction results using (b) k-t FOCUSS with NLMC, (c) k-t SLR, and (d) the proposed algorithm, respectively. The second row represents the 80th $y-t$ slice profiles of (i) ground-truth, reconstruction results using (j) k-t FOCUSS with NLMC, (k) k-t SLR, and (l) the proposed method, respectively.

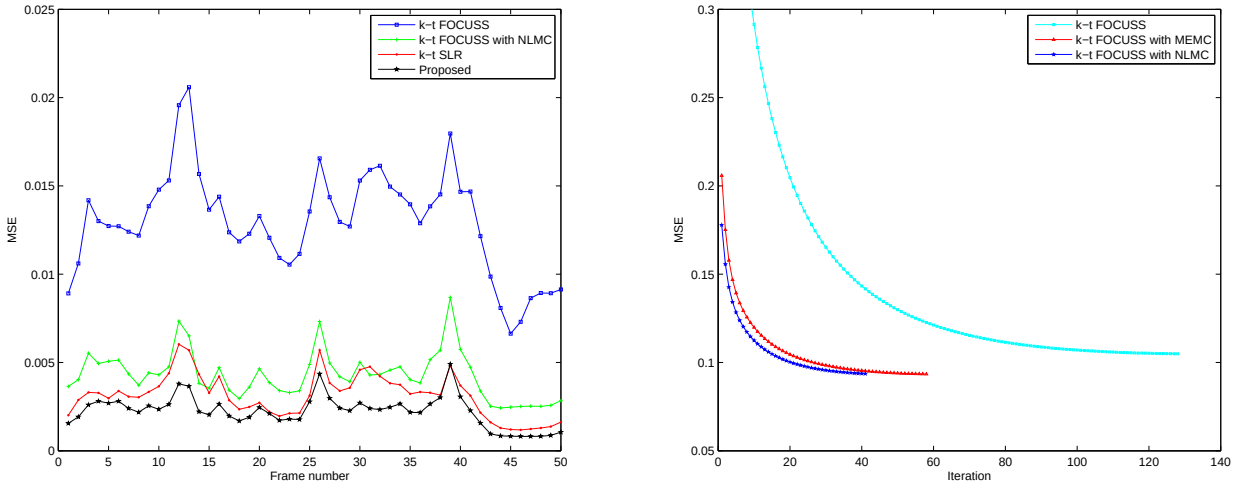

(a) MSE plot (b) Convergence plot

Figure 2: MSE and convergence plots of k-t FOCUSS, k-t FOCUSS with NLMC, k-t SLR and the proposed algorithm.

clearly reconstructed as arrows indicate. In (d) and (h), the proposed algorithm shows clearly reconstructed edge structures and we can also see that the image was highly cleansed from the noise.

Fig. 4 (a) shows MSE and convergence rate plots. We see the similar trends with the simulation data case. The proposed algorithm and k-t SLR algorithm both show lower MSE than k-t FOCUSS with NLMC. What we can see from both of visual and quantitative comparisons, the proposed algorithm has an advantage for reconstructing geometric structures in ROI important for clinical uses. Fig. 4(b) supports the assertion that

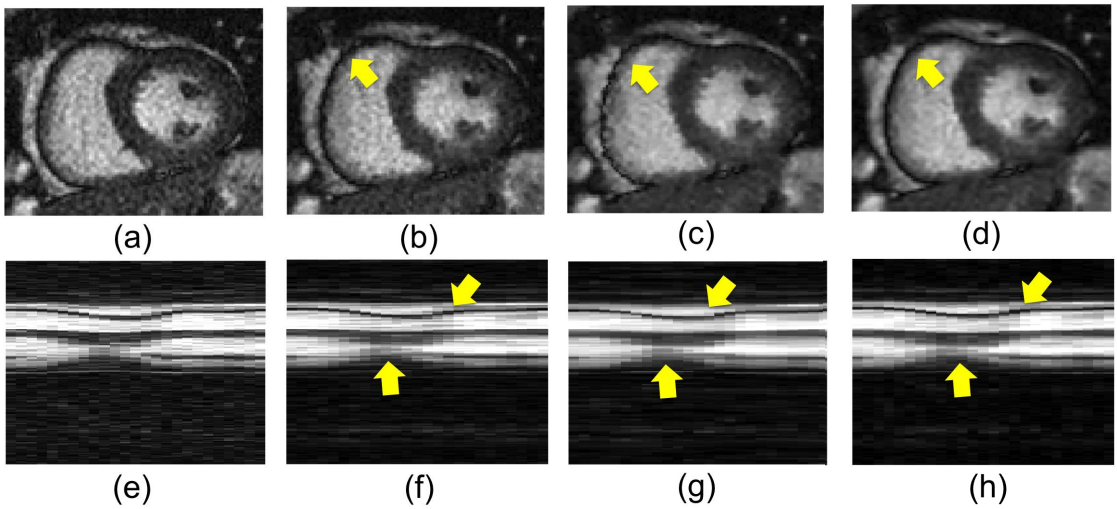

Figure 3: Reconstruction results of real Cartesian cardiac data from 1.5T scanner. The k-space data was obtained in cartesian coordinates, and the acceleration ratio was x6.1. First row represents the 17th frame images of (a) the ground-truth, reconstruction results using (b) k-t FOCUSS with NLMC, (c) k-t SLR, and (d) the proposed algorithm, respectively. The second row represents the 154th $y-t$ slice profiles of (i) ground-truth, reconstruction results using (j) k-t FOCUSS with NLMC, (k) k-t SLR, and (l) the proposed method, respectively.

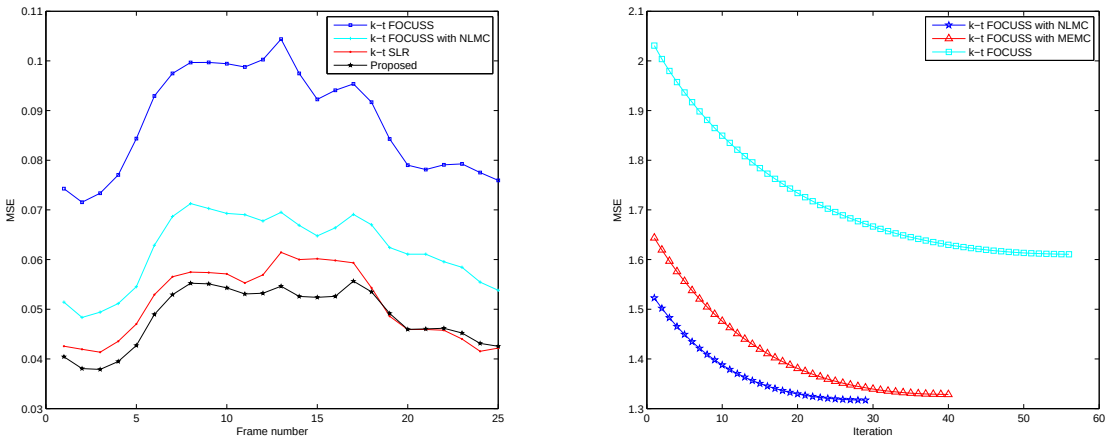

(a) MSE plot (b) Convergence plot

Figure 4: MSE and convergence plots of k-t FOCUSS, k-t FOCUSS with NLMC, k-t SLR and the proposed algorithm.

better initialization goes to better local minima with faster convergence rate.

4. DISCUSSION

To use NLMC, at least one reference frame is required. One could use a temporal averaged image during the whole acquisition time as a reference. However, due to the motion artifacts, the temporal average is often blurry, which has a negative impact on the motion compensation step. To address this, in the proposed method the

reference frame was generated by merging k-space samples during diastole phase and applying an inverse Fourier transform, since the heart is relatively stationary during this period.

Trzasko *et al.*[9] used a fast iterative shrinkage-thresholding algorithm (FISTA)[18] for patch-based rank penalty for calibration free parallel imaging (CLEAR). The main difference of CLEAR is that they exploits the low rank structure along the coil direction. To apply FISTA, patch-based SVD is need for each iteration of the gradient step. Since most of the computational complexity in our algorithm is in singular value shrinkage, the application of such a shrinkage operation for each gradient step is computationally inefficient. In our optimization framework, we firstly solve for $\mathbf{x}$ using the conjugate gradient algorithm (multiple gradient steps), after which SVD is applied. This makes the algorithm converge much faster than FISTA. Similar observations have been made using the alternating directional method of multiplier (ADMM) or the alternating augmented Lagrangian method (ALM).[14]

5. CONCLUSION

In this paper, a new reconstruction algorithm for dynamic MRI using patch-based low-rank penalty was proposed based on the observation that rank structures are relatively less sensitive to global intensity changes but make it easier to capture important structures like edges. The reconstruction problem is formulated as a variational form with non-convex generalized Huber rank penalty. To deal with the non-convex and non-smooth penalty, a difference of convex algorithm using CCCP procedure has been proposed. Experimental results show that the proposed algorithm provides clearer reconstruction than other algorithms for clinically important cardiac structures especially in ROI.

ACKNOWLEDGMENTS

This work was supported by Korea Science and Engineering Foundation, Grant number 2011-0000353.

REFERENCES

[1] Lustig, M., Santos, J., Donoho, D., and Pauly, J., "kt SPARSE: High frame rate dynamic MRI exploiting spatio-temporal sparsity," in [*Proceedings of the 13th Annual Meeting of ISMRM, Seattle*], 2420 (2006).

[2] Donoho, D. L., "Compressed Sensing," *IEEE Trans. on Information Theory* **52**, 1289–1306 (April 2006).

[3] Jung, H., Sung, K., Nayak, K., Kim, E., and Ye, J., "k-t FOCUSS: A general compressed sensing framework for high resolution dynamic MRI," *Magnetic Resonance in Medicine* **61**(1), 103–116 (2009).

[4] Ravishankar, S. and Bresler, Y., "MR image reconstruction from highly undersampled k-space data by dictionary learning," *IEEE Trans. on Medical Imaging* **30**(5), 1028–1041 (2011).

[5] Akçakaya, M., Basha, T., Goddu, B., Goepfert, L., Kissinger, K., Tarokh, V., Manning, W., and Nezafat, R., "Low-dimensional-structure self-learning and thresholding (LOST) : Regularization beyond compressed sensing for MRI reconstruction.," *Magnetic Resonance in Medicine* **66**(3), 756–767 (2011).

[6] Yang, Z. and Jacob, M., "A unified energy minimization framework for nonlocal regularization," in [*IEEE International Symposium on Biomedical Imaging: From Nano to Macro,2011*], 1150–1153, IEEE (2011).

[7] Yang, Z. and Jacob, M., "Robust non-local regularization framework for motion compensated dynamic imaging without explicit motion estimation," in [*IEEE International Symposium on Biomedical Imaging (ISBI), Barcelona*], (2012).

[8] Yang, Z. and Jacob, M., "Nonlocal regularization of inverse problems: a unified variational framework," *IEEE transactions on image processing: a publication of the IEEE Signal Processing Society* (2012).

[9] Trzasko, J. and Manduca, A., "Calibrationless parallel MRI using CLEAR," in [*IEEE Signals, Systems and Computers (ASILOMAR)*], 75–79 (2011).

[10] Candès, E. and Recht, B., "Exact matrix completion via convex optimization," *Foundations of Computational mathematics* **9**(6), 717–772 (2009).

[11] Chartrand, R., "Nonconvex splitting for regularized low-rank+ sparse decomposition," *Los Alamos National Laboratory Report: LA-UR-11-11298* (2012).

[12] Yuille, A. and Rangarajan, A., "The concave-convex procedure," *Neural Computation* **15**(4), 915–936 (2003).

[13] Chartrand, R. and Staneva, V., "Restricted isometry properties and nonconvex compressive sensing," *Inverse Problems* **24**(3), 035020 (2008).
[14] Afonso, M., Bioucas-Dias, J., and Figueiredo, M., "An augmented Lagrangian approach to the constrained optimization formulation of imaging inverse problems," *IEEE Trans. on Image Processing* **20**(3), 681–695 (2011).
[15] Lingala, S. G., Hu, Y., DiBella, E., and Jacob, M., "Accelerated dynamic MRI exploiting sparsity and low-rank structure: kt SLR," *IEEE Transactions on Medical Imaging* **30**(5), 1042–1054 (2011).
[16] Segars, W. P., Lalush, D. S., and Tsui, B. M., "A realistic spline-based dynamic heart phantom," *IEEE Transactions on Nuclear Science* **46**(3), 503–506 (1999).
[17] Segars, W. P., Lalush, D. S., and Tsui, B. M., "Modeling respiratory mechanics in the mcat and spline-based mcat phantoms," *IEEE Transactions on Nuclear Science* **48**(1), 89–97 (2001).
[18] Beck, A. and Teboulle, M., "A fast iterative shrinkage-thresholding algorithm with application to wavelet-based image deblurring," in [*IEEE International Conference on Acoustics, Speech and Signal Processing, 2009*], 693–696 (2009).